CO_2 reforming with methane for syngas production using a dielectric barrier discharge plasma coupled with Ni/γ-Al_2O_3 catalysts: process optimization through response surface methodology

D. H. Mei, S. Y. Liu, X. Tu*

Department of Electrical Engineering and Electronics, University of Liverpool, Brownlow Hill, Liverpool, L69 3GJ, UK

* Corresponding author

Dr. Xin Tu

Department of Electrical Engineering and Electronics

University of Liverpool

Liverpool L69 3GJ

UK

E-mail: xin.tu@liverpool.ac.uk

Graphic abstract

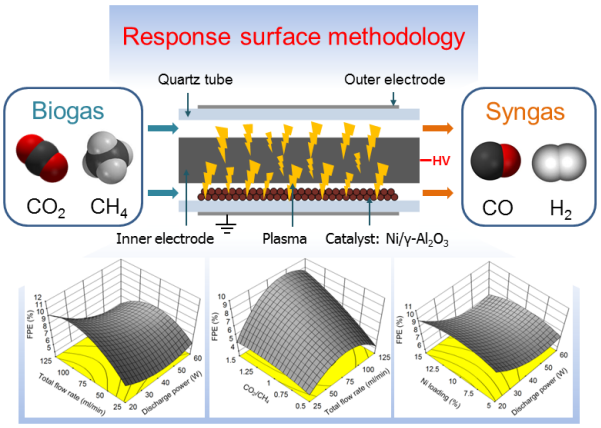

Abstract

In this work, CO_2 reforming with methane in the form of biogas over Ni/γ-Al_2O_3 catalysts was carried out in a coaxial dielectric barrier discharge (DBD) non-thermal plasma reactor. The effects of various process parameters (biogas flow rate, discharge power, CO_2/CH_4 molar ratio and Ni loading) and their interactions on the hybrid plasma-catalytic biogas reforming were evaluated using response surface methodology through a four-factor, five-level central composition design. Quadratic regression models were developed to gain a better understanding of the relationships between these process parameters (independent variables) and the biogas conversion, syngas yield and energy efficiency (responses) of the plasma reforming process. The results indicated that biogas flow rate was the most significant factor affecting the conversion of CO_2 and CH_4 and syngas yield, while the CO_2/CH_4 molar ratio was the leading process parameter determining the energy efficiency of the process. In addition, there was a trade-off between the biogas conversion and energy efficiency of the process at different specific energy inputs (SEI). The process optimization suggested that the optimal process performance was achieved at a biogas flow rate of 56.1 ml/min, a discharge power of 60.0 W, a CO_2/CH_4 molar ratio of 1.03 and a Ni loading of 9.5 wt.%, which was demonstrated by the reproducibility of the experimental results. Moreover, the carbon deposition on the spent catalyst was only 3.9% after running the plasma biogas reforming process for 150 min under the optimum experimental conditions.

Keywords

Biogas reforming; CO_2 conversion and utilization; response surface methodology; dielectric barrier discharge; plasma-catalysis; process optimization

1. Introduction

Biogas is a renewable and sustainable energy source, containing a mixture of CH_4, CO_2 and other trace components (e.g., H_2S, NH_3 and water vapor). Biogas can be used for the generation of heat, steam and electricity [1]. Biogas energy recovery for the production of both electricity and heat has significantly increased in the EU. For example, in 2011 over 18.2% of the total electricity consumed in the EU was produced from biogas [2].

With minor purification, biogas can be converted to syngas (a mixture of H_2 and CO) via a reforming process (Eq. (1)). Syngas is a key chemical feedstock for the production of oxygenated compounds (e.g. alcohols and acetic acid) and for Fischer-Tropsch synthesis to produce liquid hydrocarbons [3]. Biogas reforming is considered an attractive direct synthetic route for biogas utilization as there is no need for prior CO_2 separation, which can be costly [4]. In addition, syngas is produced from the two most abundant greenhouse gases (CO_2 and CH_4), which can provide a renewable energy source with a potential carbon footprint of zero and reduce the emission of greenhouse gases into atmosphere. Nevertheless, thermal catalytic biogas reforming on a commercial scale is limited due to the high energy cost incurred by the strongly endothermic reaction and catalyst deactivation caused by carbon deposition, especially at a high CH_4/CO_2 molar ratio.

$$CH_4 + CO_2 \rightarrow 2H_2 + 2CO \qquad \Delta H = 247 \text{ kJ/mol} \tag{1}$$

Non-thermal plasma is regarded as a promising alternative to the thermal catalytic process due to its unique non-equilibrium characteristics [5-9]. In non-thermal plasmas, the bulk gas temperature remains low, while the electrons are highly energetic with an average electron temperature of 1- 10 eV, which can activate reactant molecules by electron impact excitation, ionization and dissociation. Moreover, the combination of non-thermal plasma and catalysts (plasma-catalysis) has great potential to generate synergy, which can lower the operating temperature of catalysts and improve their catalytic activity and stability, thereby significantly enhancing the conversion of reactants, yield and selectivity of desired products and the process energy efficiency. Various non-thermal

plasma sources have been applied for biogas reforming, such as dielectric barrier discharges (DBDs) [10-13], gliding arc discharges [14-16], glow discharges [17, 18] and corona discharges [19, 20]. Among them, DBD has attracted increasing interest for the synthesis of fuels and chemicals at low temperatures due to its simple design and up-scaling capability [21]. Furthermore, catalysts can be easily integrated into a DBD reactor as a hybrid process to generate a synergistic effect of plasma-catalysis, improving the selectivity of the desired products [11, 22]. Ni/Al_2O_3 is the most commonly used catalyst in the plasma-catalytic dry reforming of methane [10-12, 23-25]. The plasma-catalytic synergy has been observed when placing a Ni/Al_2O_3 catalyst in a cylindrical DBD reactor [11], in which both the conversion of biogas and the yield of target products were significantly enhanced, compared to the reaction using plasma alone or catalysis alone at the same low temperature.

Plasma-catalytic biogas reforming for the synthesis of value-added fuels and chemicals involves a large number of physical and chemical reactions. The performance of the hybrid plasma process is determined by a range of process parameters [26, 27]. Previous works on plasma-catalytic chemical reactions have been based on standard experimental approaches [11, 12], which look at the influence of only one of these process parameters in isolation from the others each time. It is time consuming and labor intensive to screen a large number of process parameters to get a full picture of the plasma process using this conventional method; and the relative importance of different parameters on the hybrid process, especially the interactive effects of two or more parameters, cannot be clearly understood. Plasma chemical kinetic modeling offers a potential alternative approach to optimize and maximize the reaction performance of the plasma process [28-31]. Although the model calculation can be fast depending on the model details, developing a comprehensive model takes time; thus, it is not always useful for fast and cost-effective optimization of a highly complex plasma chemical process, especially when catalysts are coupled with the plasma as a hybrid plasma-catalytic process. Recently, response surface methodology (RSM) has been widely used in process optimization due to its versatility for various complex processes [32]. As a mathematical and statistical technique, RSM is commonly used to design

experiments, develop optimization models, evaluate variable effects and determine the optimum levels of independent variables within the design space that produce targeted responses with fewer experiments in less time. In addition, RSM can provide information on the effects of individual independent variables and the interactions of these parameters on the responses by three-dimensional response surface plots and two-dimensional contours interpretations. So far very limited work has been devoted to the investigation of plasma chemical processes using DoE approach [26, 27], while the use of DoE for quick optimization of hybrid plasma-catalytic processes (e.g. biogas reforming) has not been done before.

In this paper, we reported the coupling of the plasma with Ni/γ-Al_2O_3 catalysts for the reforming of CO_2 and CH_4 in the form of simulated biogas in a coaxial DBD reactor. The effects of the discharge power, total flow rate, CO_2/CH_4 molar ratio and Ni loading on the plasma-catalytic process were investigated. The RSM based on the central composite design (CCD) was used to understand the relationship between these key variables and the process performance of the plasma-catalytic reaction, and to optimize the hybrid process in terms of the conversion of biogas, product yields and fuel production efficiency (FPE) of the plasma process. In addition, the effects of different process parameters and their interactions on the reaction performance were discussed.

2. Experimental

2.1 Catalyst preparation and characterization

The *x* wt.% Ni/γ-Al_2O_3 catalysts (*x* = 5, 7.5, 10, 12.5 and 15) were prepared by wetness impregnation method, as detailed in our previous work [10]. N_2 adsorption-desorption isotherms were carried out to measure the surface properties of the catalysts. XRD patterns of the catalysts were determined by an X-ray diffractometer (Rigaku, SmartLab) equipped with Cu-Kα radiation (tube voltage 40 kV and tube current 40 mA) in the scanning range 2θ from 10^o to 80^o. Carbon deposition on the spent catalysts was analyzed by the TGA in air atmosphere using a TA Instruments SDT-Q600.

2.3 Experimental setup

Biogas reforming was carried out in a coaxial DBD non-thermal plasma reactor. The details of the DBD reactor can be found in our previous work [10]. A mixture of CO_2 and CH_4 was used as the simulated biogas. 0.5 g of Ni catalyst (1 mm in diameter) was placed along the bottom of the DBD reactor in the discharge zone. Prior to the plasma-catalytic biogas reforming, the Ni catalyst was reduced by an Ar-H_2 plasma at a discharge power of 50 W and a total flow rate of 50 ml/min with 20 vol.% H_2 for 30 min in the same DBD reactor. The DBD reactor was connected to an AC high voltage power supply with a maximum peak voltage of 30 kV and a frequency range of 5-20 kHz. All the electrical signals (applied voltage, current and voltage on the external capacitor) were recorded by a digital oscilloscope (TDS2014). The discharge power was calculated using the *Q*-*U* Lissajous figure. A homemade online power measurement system was used to control the discharge power in real time.

The specific energy input (SEI) of the plasma process was determined by

$$\mathrm{SEI(kJ/l)} = \frac{60 \times \text{Discharge power (W)}}{\text{Total feed flow rate (ml/min)}} \tag{2}$$

The gas products were analyzed by a gas chromatograph (Shimadzu GC-2014) equipped with a flame ionization detector and a thermal conductivity detector. CO_2 conversion, CH_4 conversion and total carbon conversion were defined as

$$\mathrm{C_{CO_2}(\%)} = \frac{\mathrm{CO_2\ converted\ (mol/s)}}{\mathrm{CO_2\ input\ (mol/s)}} \times 100 \tag{3}$$

$$\mathrm{C_{CH_4}(\%)} = \frac{\mathrm{CH_4\ converted\ (mol/s)}}{\mathrm{CH_4\ input\ (mol/s)}} \times 100 \tag{4}$$

$$\mathrm{C_{TC}(\%)} = x_{CO_2} \times C_{CO_2} + x_{CH_4} \times C_{CH_4} \tag{5}$$

where x_{CO_2} and x_{CH_4} were the concentration (%) of CO_2 and CH_4 in the gas, respectively.

The yield (Y) of H_2 and CO was calculated by

$$Y_{H_2}(\%) = \frac{H_2 \text{ produced (mol/s)}}{2 \times CH_4 \text{ input (mol/s)}} \times 100 \quad (6)$$

$$Y_{CO}(\%) = \frac{CO \text{ produced (mol/s)}}{CH_4 \text{ input (mol/s)} + CO_2 \text{ input (mol/s)}} \times 100 \quad (7)$$

The fuel production efficiency (FPE) of the process was determined by:

$$FPE(\%) = \frac{\sum \text{fuel produced (mol/s)} \times \text{LHV(kJ/mol)}}{CH_4 \text{converted (mol/s)} \times \text{LHV of } CH_4 \text{(kJ/mol)} + \text{Discharge power (kW)}} \times 100 \quad (8)$$

where LHV is the low heating value of the fuel [10].

2.3Response surface methodology

A four-factor and five-level CCD based RSM was developed to understand the effects of each process parameter and their interactions on the hybrid plasma-catalytic process. Four parameters, including discharge power (X_1), total flow rate (X_2), CO_2/CH_4 molar ratio (X_3), and Ni loading (X_4) were chosen as the independent variables for the design based on our previous works [11, 23]. In this experiment, syngas was the major product, while a small amount of saturated hydrocarbons such as ethane, propane and butane were also detected in the gas products. Therefore, only syngas was considered as the major gas product in the following model, while CO_2 conversion (Y_1), CH_4 conversion (Y_2), CO yield (Y_3), H_2 yield (Y_4) and FPE (Y_5) were identified as the responses in this work. Each process parameter has five levels of -2, -1, 0, +1 and +2 according to the following equation,

$$x_i = \frac{X_i - X_o}{\Delta X_i} \quad (9)$$

where x_i and X_i are the coded and actual value of the i^{th} parameter, respectively. X_0 is the value of the i^{th} parameter at the center point within the tested range and ΔX_i is the step size. The coded and actual levels of the process parameters are given in Table 1.

Table 1 Independent variables with coded and actual values in CCD.

Independent variables	Unit	Coded factors	Levels and ranges

			-2	-1	0	+1	+2
Discharge power (X_1)	W	x_1	20	30	40	50	60
Total flow rate (X_2)	ml/min	x_2	25	50	75	100	125
CO_2/CH_4molar ratio (X_3)	-	x_3	0.5	0.75	1	1.25	1.5
Ni loading (X_4)	wt.%	x_4	5	7.5	10	12.5	15

In the CCD design, the relationship between the process parameters and output responses can be expressed by second-order regression models. The general form of the second-order polynomial equation was defined as follows [33]:

$$Y = \beta_0 + \sum_{i=1}^{4} \beta_i x_i + \sum_{i=1}^{4} \beta_{ii} x_{ii}^2 + \sum_{i=1}^{3} \sum_{j=i+1}^{4} \beta_{ij} x_i x_j \quad (10)$$

where Y and x_i are the response and the coded value of the independent variables, respectively. β_0 is a constant coefficient, whilst β_i, β_{ii} and β_{ij} are linear, quadratic and interactions coefficients, respectively.

The adequacy and fit of the models can be determined by the analysis of variance (ANOVA). The statistical significance of the models and of each term can be identified by the F-test and adequacy measurements such as the coefficient of determination R^2, adjusted R^2 and predicted R^2. The difference between the predicted $R^2$and adjusted R^2 should be < 0.2 for a well-developed model [33]. The above analysis was conducted using a Design Expert software version 10 (trial version) [34]. The interactions of the process parameters were examined by the responses surface and contour plots from the regression models.

3. Results and discussion

3.1 Catalyst characterization

Table 2 shows the physicochemical properties of the catalysts and support. The specific surface area of γ-Al_2O_3 was 299.8 m^2/g. Increasing the Ni loading from 5 wt.% to 15 wt.% decreased the specific surface area of the Ni catalysts from 294.0 to 223.9 m^2/g. The total pore volume of the Ni

catalysts was slightly lower than that of γ-Al_2O_3, while the average pore diameter of the catalysts was larger than that of the support. Similar findings were reported by Han et al. using Ni/Al_2O_3 catalysts for thermal-catalytic CO_2 reforming of CH_4 in fixed-bed and fluidized bed reactors [35].

Table 2 Physicochemical properties of the fresh catalyst.

Sample	S_{BET} (m^2/g)	Total pore volume (cm^3/g)	Average pore diameter (nm)
γ-Al_2O_3	299.8	0.45	3.60
5Ni	294.0	0.43	3.63
7.5Ni	274.9	0.42	3.75
10Ni	268.0	0.39	3.80
12.5Ni	249.9	0.35	3.83
15Ni	223.9	0.34	3.84

Fig. 1 shows the XRD patterns of the fresh catalysts and γ-Al_2O_3. The XRD pattern of γ-Al_2O_3 showed five major crystalline peaks with cubic structure (2θ =14.5°, 28.3°, 38.5 °, 49.7 ° and 67.1°, PDF # 52-0803). The peaks of NiO (2θ = 37.2° and 43.3°, PDF # 44-1159) were detected in the XRD pattern of the Ni catalysts. The intensity of the NiO peak at 2θ = 43.3° was increased with the Ni loading, which indicates the formation of larger NiO particles due to aggregation at high Ni loadings [35]. Previous work showed that NiO/Al_2O_3 can be reduced and activated by plasmas in a mixture of Ar and H_2 for further catalytic reaction [36].

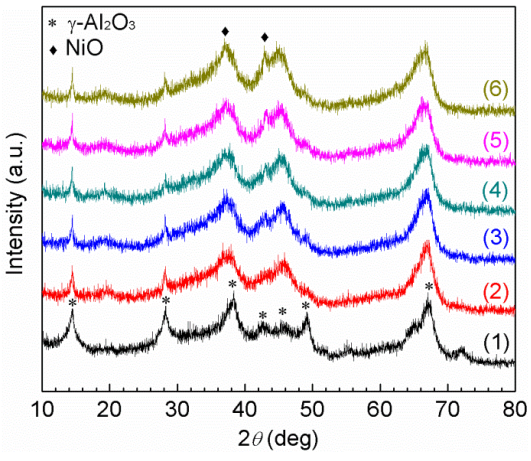

Fig. 1. XRD patterns of fresh catalyst with different Ni loadings: (1) γ-Al_2O_3; (2) 5Ni; (3) 7.5Ni; (4) 10Ni; (5) 12.5Ni; (6) 15Ni.

3.2 DoE analysis

3.2.1 Regression models

Table 3 shows the design of experiments. 30 groups of process parameters were required for the CCD design, including 6 replicated experimental runs (No. 7, 11, 13, 19, 23 and 27). The relationships between the process parameters and the output responses were established by the quadratic models, as shown in Equations (11) to (15).

Table 3 Experimental design matrix and results of the CCD.

Exp. order	Independent variables (X)				Responses (Y)				
	X_1: Discharge power (W)	X_2: Total flow rate (ml/min)	X_3: CO_2/CH_4 molar ratio	X_4: Ni loading (wt.%)	Y_1: CO_2 conversion (%)	Y_2: CH_4 conversion (%)	Y_3: CO yield (%)	Y_4: H_2 yield (%)	Y_5: Fuel production efficiency (%)
1	40	75	1	15	18.1	25.4	11.0	9.0	7.5
2	20	75	1	10	15.5	21.0	9.8	7.3	11.3
3	40	75	1.5	10	16.3	37.2	15.9	13.0	9.4
4	40	75	0.5	10	23.1	20.2	8.5	6.9	6.6
5	30	100	1.25	7.5	11.2	22.2	9.7	7.5	10.0
6	50	100	1.25	12.5	19.1	33.1	14.2	12.0	8.2
7[a)]	40	75	1	10	20.3	28.7	12.8	10.1	8.3
8	30	100	0.75	7.5	14.0	14.3	6.6	4.6	7.7
9	50	50	1.25	7.5	26.5	48.1	20.3	17.4	7.3
10	40	75	1	5	18.7	26.9	11.4	9.4	7.7
11[b)]	40	75	1	10	20.5	29.3	12.6	10.2	8.2
12	50	100	0.75	12.5	18.6	21.9	8.4	6.8	6.5
13[c)]	40	75	1	10	20.5	29.2	12.7	10.3	8.3
14	50	100	0.75	7.5	19.1	21.8	8.6	7.0	6.7
15	50	50	0.75	7.5	31.7	36.6	16.3	13.9	6.6
16	50	100	1.25	7.5	15.1	31.4	11.8	9.7	7.9
17	40	25	1	10	31.0	44.0	19.1	16.6	5.4

18	50	100	1.25	12.5	14.8	30.5	11.5	9.3	7.8
19[d)]	40	75	1	10	20.6	29.3	12.4	10.2	8.1
20	30	100	0.75	12.5	13.6	14.2	6.5	4.5	7.6
21	30	100	1.25	12.5	11.0	20.7	9.4	7.2	9.8
22	50	50	0.75	12.5	30.9	35.5	15.9	13.5	6.5
23[e)]	40	75	1	10	20.4	29.4	12.9	10.2	8.5
24	40	125	1	10	10.5	17.5	7.1	4.8	7.3
25	30	50	0.75	7.5	23.6	25.6	11.0	9.4	7.2
26	30	50	1.25	7.5	19.6	38.4	14.6	12.5	8.2
27[f)]	40	75	1	10	20.4	29.8	12.4	10.3	8.2
28	60	75	1	10	27.0	41.2	18.4	14.6	8.1
29	50	50	1.25	12.5	25.8	46.0	19.8	16.9	7.1
30	30	50	0.75	12.5	23.0	24.2	10.7	9.1	7.1

a)-f) Replicated experimental runs (run order: 7, 11, 13, 19, 23 and 27).

Y_1: CO_2 conversion (%)

$$= +20.45 + 2.93x_1 - 5.15x_2 - 1.88x_3 - 0.22x_4 - 0.74x_1x_2 - 0.30x_1x_3 - 0.042x_1x_4 + 0.31x_2x_3 + 0.073x_2x_4 + 0.029x_3x_4 + 0.16x_1^2 + 0.051x_2^2 - 0.22x_3^2 - 0.55x_4^2 \quad (11)$$

Y_2: CH_4 conversion (%)

$$= +29.28 + 5.00x_1 - 6.83x_2 + 4.59x_3 - 0.65x_4 - 0.65x_1x_2 + 0.25x_1x_3 + 0.27x_1x_4 - 0.68x_2x_3 + 0.46x_2x_4 - 0.46x_3x_4 + 0.42x_1^2 + 0.34x_2^2 - 0.17x_3^2 - 0.80x_4^2 \quad (12)$$

Y_3: CO yield (%)

$$= +12.61 + 1.97x_1 - 3.11x_2 + 1.76x_3 - 0.14x_4 - 0.86x_1x_2 + 0.081x_1x_3 - 0.017x_1x_4 - 0.16x_2x_3 + 0.038x_2x_4 - 0.031x_3x_4 + 0.30x_1^2 + 0.054x_2^2 - 0.18x_3^2 - 0.43x_4^2 \quad (13)$$

Y_4: H_2 yield (%)

$$= +10.22 + 1.77x_1 - 2.99x_2 + 1.49x_3 - 0.14x_4 - 0.61x_1x_2 + 0.030x_1x_3 - 0.026x_1x_4 - 0.14x_2x_3 + 0.050x_2x_4 - 0.033x_3x_4 + 0.17x_1^2 + 0.097x_2^2 - 0.091x_3^2 - 0.27x_4^2 \quad (14)$$

Y_5: FPE (%)

$$= +8.26 - 0.66x_1 + 0.43x_2 + 0.67x_3 - 0.065x_4 - 0.20x_1x_2 + 0.17x_1x_3 - 2.68\times10^{-3}x_1x_4 + 0.22x_2x_3 - 0.012x_2x_4 - 2.206\times10^{-3}x_3x_4 + 0.31x_1^2 + 0.097x_2^2 - 0.10x_3^2 - 0.21x_4^2 \quad (15)$$

The significance and adequacy of the regression models were determined by the ANOVA. Table 4 shows the ANOVA results of the quadratic model for each response based on the data in Table S1-S5 in Supporting information. The *F*-values for the responses Y_1 to Y_5 are higher compared to

the critical value of 2.43 in this work [33], which indicates that the regression models are statistically significant. In addition, the low *p*-values (<0.0001) indicate that the significance of all models is at a confidence level of > 95%. The high *F*-values and low *p*-values confirm that most variations in the responses can be explained by the regression models. The coefficient of determination R^2 for each model is close to 1, which indicates the experimental data agrees with the predicted results calculated by the regression models. For all the responses, the predicted R^2 fits well with the adjusted R^2, showing the stability and validity of the regression models. These results show that all the regression models are statistically significant and adequate for the prediction and optimization of the plasma-catalytic biogas reforming process.

Table 4 Summary of the ANOVA for the quadratic model of each response.

Response	*F*-value	*p*-value	R^2	Adjusted R^2	Predicted R^2	Model term with highest *F*-value	Model terms with *p*-value < 0.05
Y_1: CO_2 conversion	1432.55	<0.0001	0.9993	0.9886	0.9862	x_2	x_1, x_2, x_3, x_4, x_1x_2, x_1x_3, x_2x_3, x_1^2, x_3^2, x_4^2
Y_2: CH_4 conversion	403.39	<0.0001	0.9874	0.9849	0.9643	x_2	x_1, x_2, x_3, x_4, x_1x_2, x_2x_3, x_2x_4, x_3x_4, x_1^2, x_2^2, x_4^2
Y_3: CO yield	231.52	<0.0001	0.9954	0.9841	0.9756	x_2	x_1, x_2, x_3, x_1x_2, x_1^2, x_3^2, x_4^2
Y_4: H_2 yield	1309.88	<0.0001	0.9913	0.9884	0.9658	x_2	x_1, x_2, x_3, x_4, x_1x_2, x_2x_3, x_1^2, x_2^2, x_3^2, x_4^2
Y_5: Fuel production efficiency	48.66	<0.0001	0.9785	0.9583	0.9154	x_3	x_1, x_2, x_3, x_1x_2, x_1x_3, x_2x_3, x_1^2, x_2^2, x_3^2, x_4^2

3.2.2 Effect of plasma processing parameters on the conversion of biogas

If the *p*-value of a model term (individual process parameter or interaction of two parameters) is below the level of significance (0.05 in this work), the corresponding term is considered important to the plasma process. In the plasma-catalytic biogas reforming, x_1, x_2, x_3, x_4, x_1x_2, x_1x_3, x_2x_3, x_1^2, x_3^2, x_4^2 are identified as significant terms for CO_2 conversion, while x_1, x_2, x_3, x_4, x_1x_2, x_2x_3, x_2x_4, x_3x_4, x_1^2,

198 x_2^2, x_4^2 are important for CH_4 conversion. The relative importance of a model term is associated to
199 its *F*-value. The total biogas flow rate has been identified as the most important parameter for the
200 conversion of both CO_2 and CH_4 due to the highest *F*-values of 13417.53 and 2760.71, respectively
201 (shown in Table 4, Table S1 and S2 in Supporting information).

202 The effect of different process parameters and their interactions on the hybrid plasma-catalytic
203 biogas reforming are presented in terms of three-dimensional response surfaces and projected two
204 dimensional contours derived from the regression equations (Equation S1 to S5 in Supporting
205 information). Fig. 2 shows the combined effect of plasma power and total biogas flow rate on the
206 conversion of CO_2 at a CO_2/CH_4 molar ratio of 1:1 and a Ni loading of 10 wt.% (the center level).
207 The highest CO_2 conversion (~40%) can be obtained with the highest discharge power of 60 W and
208 the lowest total feed flow of 25 ml/min. Similarly, higher discharge power and lower biogas flow
209 rate contribute to the higher conversion of CH_4, as shown in Fig. S1 (Supporting information). In
210 this work, placing the Ni catalysts in the DBD reactor resulted in dominant filamentary discharges
211 due to the large void space in the plasma gap, which significantly enhanced the plasma-catalyst
212 interactions [11]. Discharge power can be controlled by changing applied voltage while keeping the
213 frequency constant. Therefore, increasing plasma power increased the number of microdischarges
214 and the current intensity in the CO_2/CH_4 DBD. As a result, more energetic electrons and reaction
215 channels can be generated in the plasma for biogas conversion [26]. Moreover, a lower total flow
216 rate contributed to the enhanced conversion of biogas due to the increased retention time of biogas
217 in the plasma reaction zone. In this study, the residence time of biogas significantly increased from
218 7.4 to 36.7 s when the total flow rate decreased from 125 to 25 ml/min, resulting in the enhanced
219 possibility of biogas activation through collisions with electrons and reactive species, thereby
220 enhancing their conversions.

221 In Fig. 2, the increasing trend of CO_2 conversion with discharge power is more remarkable at a
222 low biogas flow rate (25 ml/min), which is reflected by the larger gradient of CO_2 conversion with
223 respect to discharge power at a low biogas flow rate (Fig. 2 (b)). This suggests that the interaction

between the discharge power and biogas flow rate plays a significant role in the conversion of CO_2, as the *p*-value of the term x_1x_2 (Table S1) is less than 0.0001. Similarly, the combined effect of discharge power and total flow rate also strongly affected the conversion of CH_4, as the *p*-value of the term x_1x_2 (Table S2) is less than 0.0001.

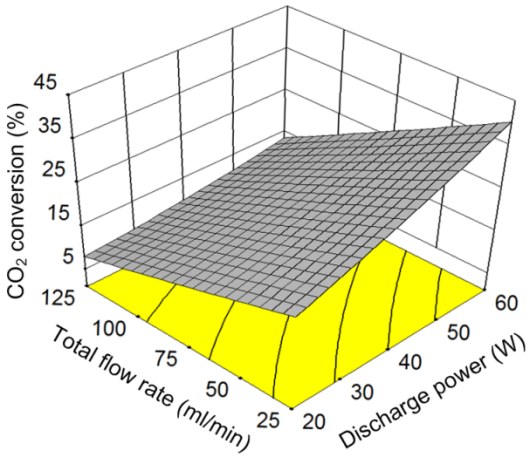

(a)

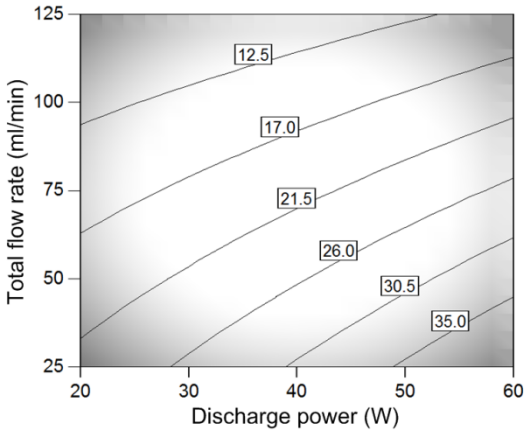

(b)

Fig. 2. Interaction between discharge power and total flow rate on CO_2 conversion at a CO_2/CH_4 molar ratio of 1:1 and a Ni loading of 10 wt.%: (a) 3D surface plot; (b) projected contour plot.

Fig. 3 shows the interactive effect of total flow rate and CO_2/CH_4 molar ratio on CO_2 conversion. The highest CO_2 conversion (around 35%) can be achieved at the lowest total flow rate (25 ml/min) and the lowest CO_2/CH_4 ratio (1:2). Increasing the ratio of CO_2/CH_4 decreased the conversion of CO_2. By contrast, increased CH_4 conversion was achieved by increasing the CO_2/CH_4 molar ratio,

as shown in Fig. S2. The highest CH_4 conversion (~55%) was achieved at the lowest biogas flow rate of 25 ml/min with a CO_2/CH_4 molar ratio of 3:2. This phenomenon was similar to that obtained in the plasma dry reforming of CH_4 without a catalyst [37]. As shown in Fig. 3 (b), CO_2 conversion was more sensitive to the change of CO_2/CH_4 molar ratio at a lower biogas flow rate compared to the reaction at a higher biogas flow rate. The gradient of CO_2 conversion with respect to CO_2/CH_4 molar ratio was -10.0% at a total gas flow rate of 25 ml/min, higher than that (-5.0%) obtained at a higher biogas flow rate of 125 ml/min. This finding suggests that the interaction between biogas flow rate and CO_2/CH_4 molar ratio is significant, which is consistent with the low *p*-value (< 0.0001) of the term x_2x_3 in Table S1. The interaction between these parameters was also considered significant on CH_4 conversion based on the low *p*-value (0.0006) of the term x_2x_3 in Table S2 and the appearance of the contour plot in Fig. S2.

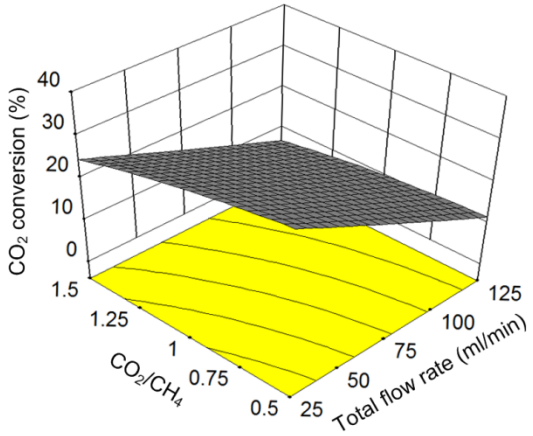

(a)

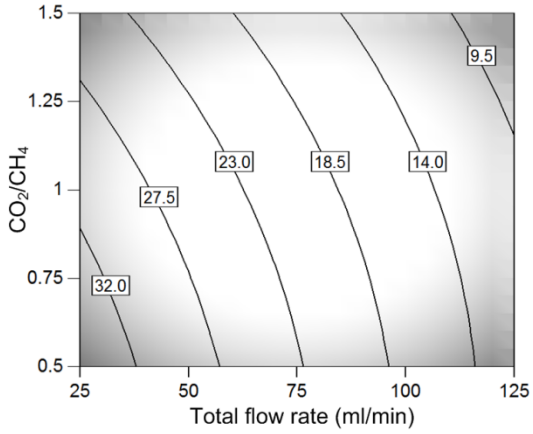

(b)

Fig. 3. Interaction between total flow rate and CO_2/CH_4 molar ratio on CO_2 conversion at a discharge power of 40 W and a Ni loading of 10 wt.%: (a) 3D surface plot; (b) projected contour plot.

The combined effect of discharge power and Ni loading on CO_2 conversion is presented in Fig. 4. An optimum Ni loading was observed to obtain a high CO_2 conversion, regardless of the discharge power. At the lower Ni loading, fewer active sites were available on the catalyst surface although a larger specific surface area was found (shown in Table 2). Therefore, CO_2 conversion initially increased with the increase of the Ni loading. However, further increasing the Ni loading led to the aggregation of metal particles (see Fig. 1) and thus decreased the specific surface area and metal dispersion [35]. These factors resulted in negative effects on the conversion of biogas. As a result, the highest CO_2 conversion was obtained at a moderate Ni loading (near 10 wt.%) at a specific discharge power. Similar phenomenon was found in the work of Mahammadunnisa et al. [23]. They used similar Ni/Al_2O_3 catalysts with different Ni contents (10 wt.%, 20 wt.% and 30 wt.%) in the plasma-catalytic CO_2 reforming of CH_4 using a DBD. Their results showed that the highest CO_2 and CH_4 conversions were obtained when using the 20 wt.% Ni/Al_2O_3 catalyst. In Fig. 4 (b), the contour lines of CO_2 conversion were almost parallel to each other, suggesting that the gradient of CO_2 conversion with respect to discharge power was nearly constant regardless of Ni loading. This indicates the insignificant role of the interaction between discharge power and Ni loading on CO_2 conversion.

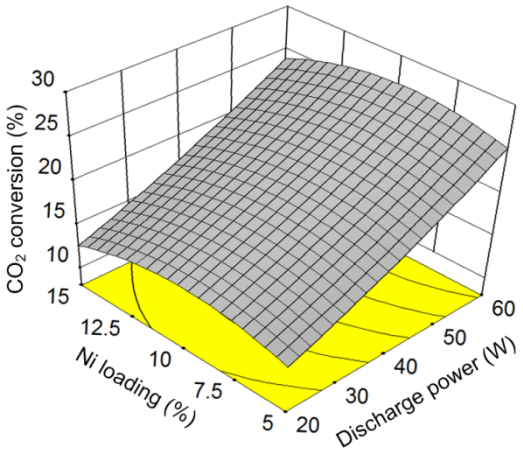

(a)

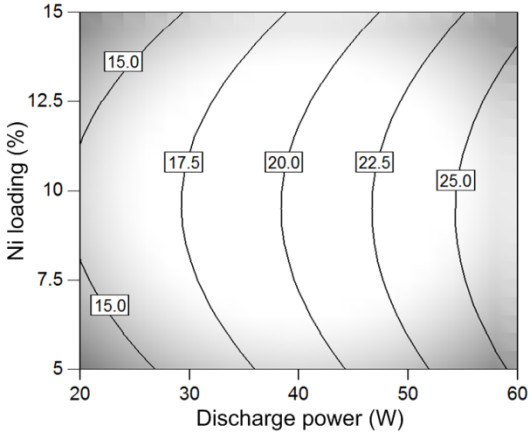

(b)

Fig. 4. Interaction between discharge power and Ni loading on CO_2 conversion at a total flow rate of 75 ml/min and a CO_2/CH_4 molar ratio of 1:1: (a) 3D surface plot; (b) projected contour plot.

The interactions of Ni loading and total flow rate with CO_2/CH_4 molar ratio were also regarded as having an insignificant effect on CO_2 conversion, which can be confirmed by their high *p*-values (0.2007 for x_2x_4 and 0.6047 for x_3x_4), as listed in Table S1. This is different to their effects on CH_4 conversion. Fig. 5 shows the interaction effect of total flow rate and Ni loading on CH_4 conversion. An optimum Ni loading was observed for higher CH_4 conversion, which was similar to the effect of the Ni loading on CO_2 conversion. This optimum Ni loading was around 7.5 wt.% at a low total flow rate of 25 ml/min and was gradually increased to a level slightly higher than 10 wt.% when the total flow rate increased to 125 ml/min. In Fig. 5(b), CH_4 conversion was found to be more sensitive to the total flow rate at a low Ni loading (5 wt.%) than that at a high Ni loading (15 wt.%). The *p*-value of the term related to the interaction of these two variables (shown in Table S2) is lower than the critical value (0.05). These results suggest that there is a significant interaction between the total biogas flow rate and Ni loading on CH_4 conversion. The optimum Ni loading for higher CH_4 conversion was also dependent on CO_2/CH_4 molar ratio, as shown in Fig. S3. At a CO_2/CH_4 molar ratio of 1:2, the optimum Ni loading was slightly higher than 10 wt.%, whereas it decreased to around 7.5 wt.% when CO_2/CH_4 molar ratio was increased to 3:2. The low *p*-value

(0.0118) of the term x_3x_4 in Table S2 suggests that the interaction between CO_2/CH_4 molar ratio and Ni loading had a significant effect on CH_4 conversion.

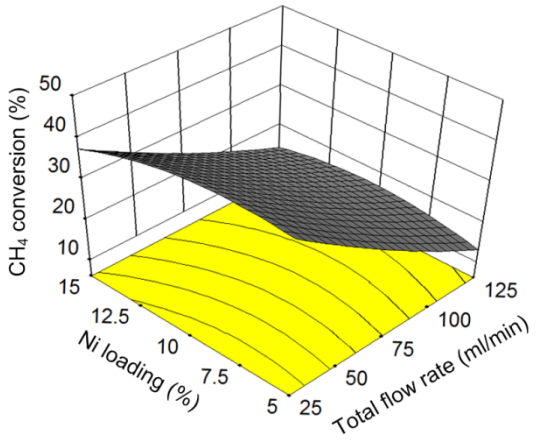

(a)

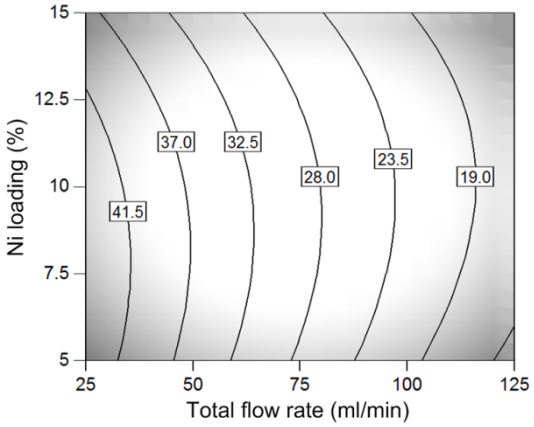

(b)

Fig. 5. Interaction between total flow rate and Ni loading on CH_4 conversion at a discharge power of 40 W and a CO_2/CH_4 molar ratio of 1:1: (a) 3D surface plot; (b) projected contour plot.

3.2.3 Effect of plasma processing parameters on the yield of CO and H_2

From the ANOVA results (see Table 2), the terms x_1, x_2, x_3, x_1x_2, x_1^2, x_3^2, x_4^2 were identified as the significant factors affecting the yield of CO, while the terms x_1, x_2, x_3, x_4, x_1x_2, x_2x_3, x_1^2, x_2^2, x_3^2, x_4^2 were important for the yield of H_2, as their low p-values were less than the critical value (0.05). The total flow rate had the most significant impact on the yield of CO and H_2, with the highest F-values of 1785.56 and 11127.16 (shown in Table S3 and S4), respectively.

Fig. 6 presents the interactive effect of discharge power and total flow rate on the yield of CO. The distorted-quadrangle response surface showed that the highest CO yield of 27.6% was obtained at a discharge power of 60 W and a total flow rate of 25 ml/min. The CO yield was enhanced by over 110% when the discharge power increased from 20 to 60 W at a total flow rate of 25 ml/min, while it only increased from 7.3% to 8.3% when raising discharge power at a total flow rate of 125 ml/min. Similarly, the gradient of CO yield with respect to biogas flow rate was much higher at a high discharge power (60 W) compared to that at a low discharge power (20 W). These phenomena suggest that the interaction between discharge power and biogas flow rate played a dominant role in determining the yield of CO, as confirmed by the appearance of the contour lines in Fig. 6 (b) and the low p-value (< 0.0001) of the term x_1x_2 in Table S3.

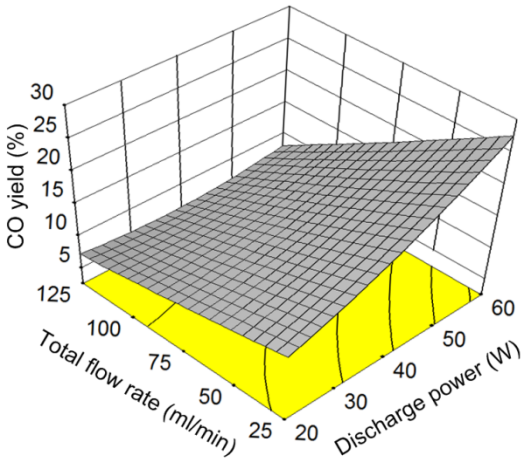

(a)

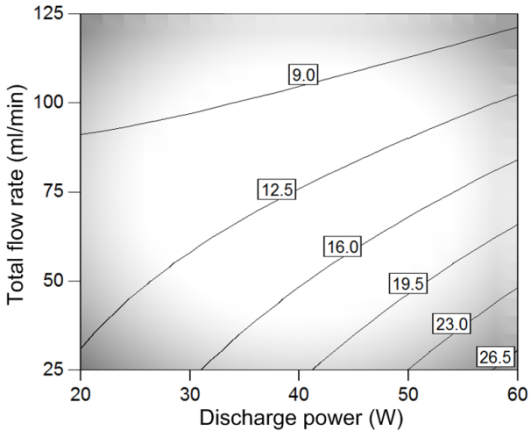

(b)

Fig. 6. Interaction between discharge power and biogas flow rate on the yield of CO at a CO_2/CH_4 molar ratio of 1:1 and a Ni loading of 10 wt.%: (a) 3D surface plot; (b) projected contour plot.

Fig. 7 shows the combined effect of the CO_2/CH_4 molar ratio and Ni loading on CO yield. An optimum Ni loading (slightly below 10 wt.%) was required to reach a high yield of CO, regardless of CO_2/CH_4 molar ratio. The yield of CO was almost independent of the Ni loading and increased by increasing the CO_2/CH_4 molar ratio from 1:2 to 3:2, as shown in Fig. 7 (b). The *p*-value (0.7333) of x_3x_4 (Table S3) was high, suggesting the combined effect of these parameters on the CO yield was weak. The interaction between CO_2/CH_4 molar ratio and Ni loading was also regarded as insignificant for the yield of H_2 as the contour lines were nearly parallel with each other in Fig. S4 (b). The high *p*-value (0.3545) of the term x_3x_4 in Table S4 also supports this conclusion. Fig. S4 also shows an optimum Ni loading for the high yield of H_2, regardless of CO_2/CH_4 molar ratio. The effect of Ni loading on the selectivity of CO and H_2 follows the same evolution as that on the selectivity of syngas.

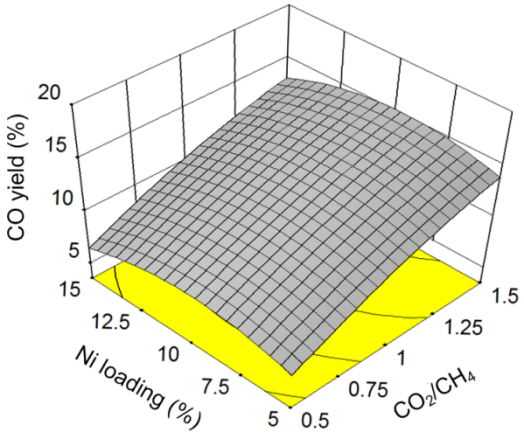

(a)

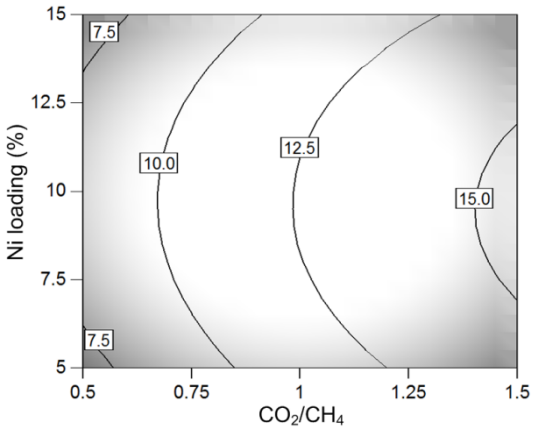

(b)

Fig. 7. Interaction between CO_2/CH_4 molar ratio and Ni loading on the yield of CO at a discharge power of 40 W and a biogas flow rate of 75 ml/min: (a) 3D surface plot; (b) projected contour plot.

Fig. 8 shows the combined effect of biogas flow rate and discharge power on the yield of H_2. The highest H_2 yield of 23.2% was achieved at the highest discharge power of 60 W and the lowest biogas flow rate of 25 ml/min. The yield of H_2 was more sensitive to the change of the biogas flow rate at a high discharge power (e.g. 60 W), as plotted in Fig. 7 (b), which suggests the presence of a significant interaction between the discharge power and biogas flow rate on the yield of H_2, as confirmed by the low p-value (< 0.0001) of the term x_1x_2 in Table S4. The low p-value of 0.0009 of the model term x_2x_3 in Table S4 indicated that the interaction effect between biogas flow rate and CO_2/CH_4 molar ratio on the H_2 yield was also significant, which is reflected by the contour lines plotted in Fig. S5.

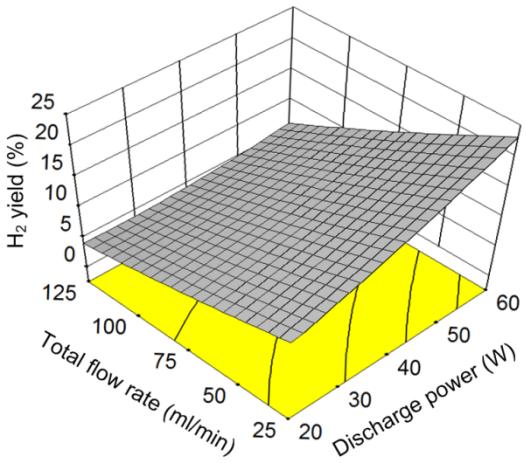

(a)

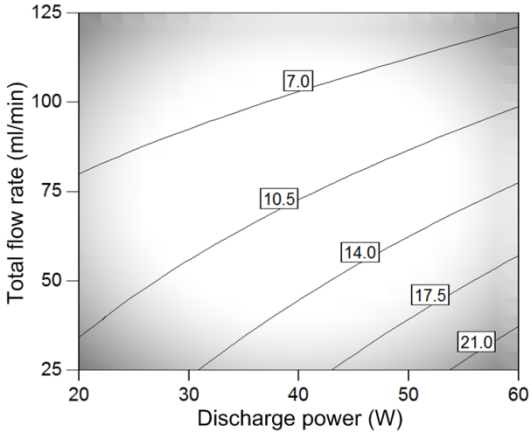

(b)

Fig. 8. Interaction between discharge power and biogas flow rate on the yield of H_2 at a CO_2/CH_4 molar ratio of 1:1 and a Ni loading of 10 wt.%: (a) 3D surface plot; (b) projected contour plot.

3.2.4 Effect of plasma processing parameters on the FPE

The terms x_1, x_2, x_3, x_1x_2, x_1x_3, x_2x_3, x_1^2, x_2^2, x_3^2, x_4^2 were identified as significant for the FPE since their *p*-values were below 0.05 (the level of significance), as shown in Table 4. Considering the highest *F*-value of 176.02 (see Table S5), the CO_2/CH_4 molar ratio can be regarded as the most important parameter determining the FPE of the process.

Fig. 9 shows the combined effect of discharge power and total feed flow rate on the FPE of the plasma process. The optimal biogas flow rate for a high energy efficiency depends on the discharge power. For example, at a discharge power of 20 W, the maximum FPE can be achieved at an optimal biogas flow rate of around 100 ml/min. However, at the higher plasma power of 60 W, the optimal biogas flow to achieve the maximum FPE was 75 ml/min. At the low (25 to 50 ml/min) and high (100 to 125 ml/min) biogas flow rates, the FPE initially decreased when increasing the discharge power and reached a peak value at a certain discharge power, beyond which the FPE increased gradually. The relationship between the discharge power and minimum FPE was also dependent on the biogas flow rate. However, at a moderate biogas flow rate (e.g. 50 to 100 ml/min), the FPE initially decreased when increasing the discharge power and stabilized when the discharge

power was higher than 45 W. The highest FPE was obtained at a discharge power of 20 W and a biogas flow rate of around 100 ml/min. The response surface had the appearance of a saddle (see Fig. 9 (b)), which indicates that the interaction between the discharge power and total feed flow rate significantly affected the FPE [38], as confirmed by the low p-value (0.0057) of the term x_1x_2 listed in Table S5.

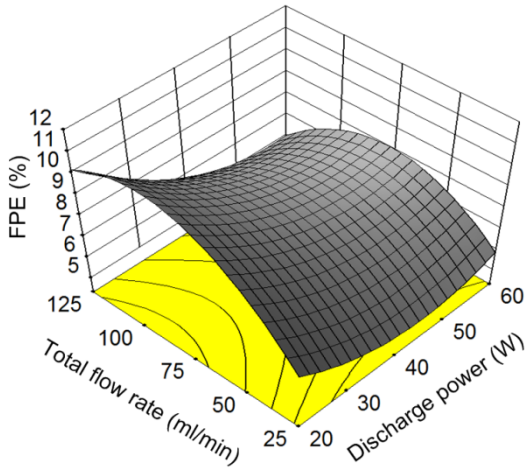

(a)

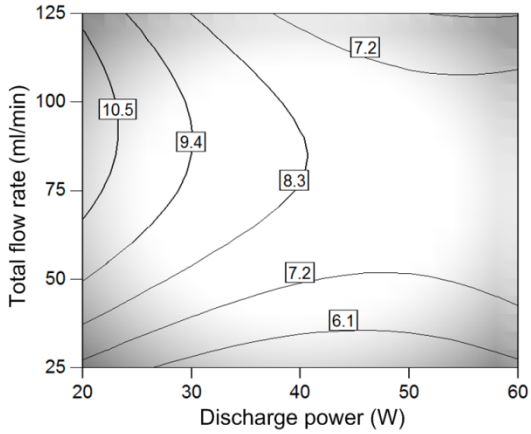

(b)

Fig. 9. Interaction between discharge power and biogas flow rate on the FPE at a CO_2/CH_4 molar ratio 1:1 and a Ni loading of 10 wt.%: (a) 3D surface plot; (b) projected contour plot.

The interactive effect of discharge power and CO_2/CH_4 molar ratio on the FPE of the hybrid process is presented in Fig. 10. The maximum FPE of around 12.4% was achieved at a discharge power of 20 W and a CO_2/CH_4 molar ratio of 3:2. When the CO_2/CH_4 molar ratio was larger than

5:4, the FPE initially decreased with the discharge power before reaching a minimum value. In addition, at a low discharge power, the FPE of the process was very sensitive to the change of CO_2/CH_4 molar ratio, as shown by the contour lines in Fig. 10 (b). Table 5S shows that the *p*-value of the term x_1x_3 (0.0126) was lower than the level of significance (0.05). These findings indicate that the interaction between discharge power and CO_2/CH_4 molar ratio plays a significant role in determining the FPE of the hybrid process. The shape of the contour lines (part of a ellipse) in Fig. 11 indicates strong interactive effects of CO_2/CH_4 molar ratio and biogas flow on the FPE, which is evidenced by the presence of low *p*-value of the term x_2x_3 (0.0029) listed in Table S5.

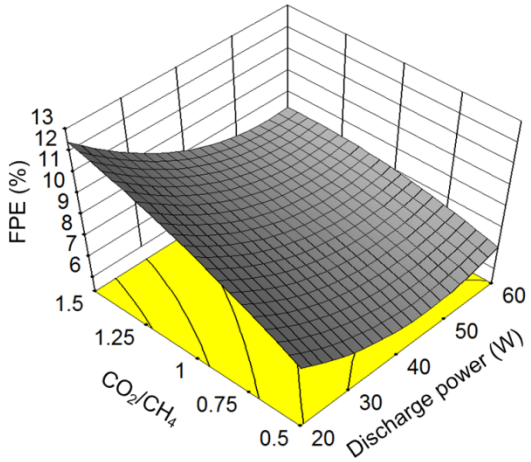

(a)

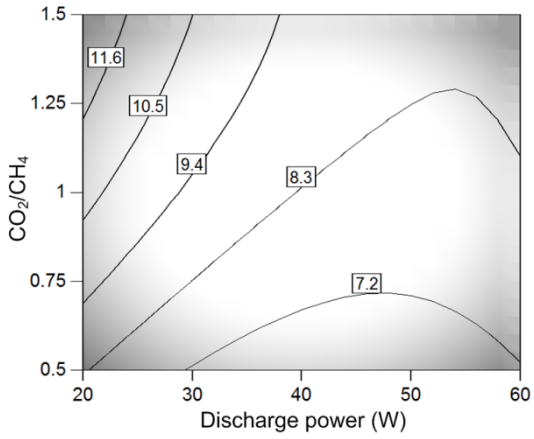

(b)

Fig. 10. Interaction between discharge power and CO_2/CH_4 molar ratio on the FPE at a biogas flow rate of 50 ml/min and a Ni loading of 10 wt.%: (a) 3D surface plot; (b) projected contour plot.

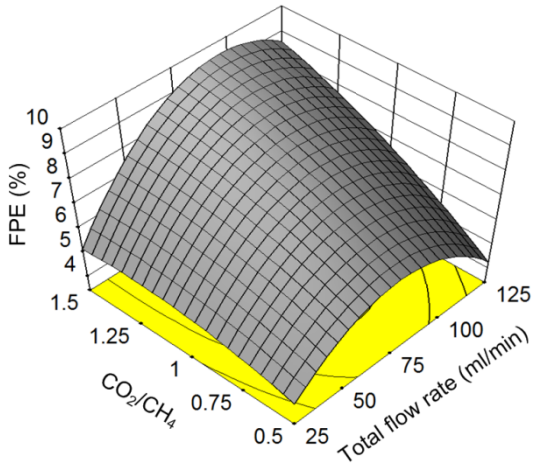

(a)

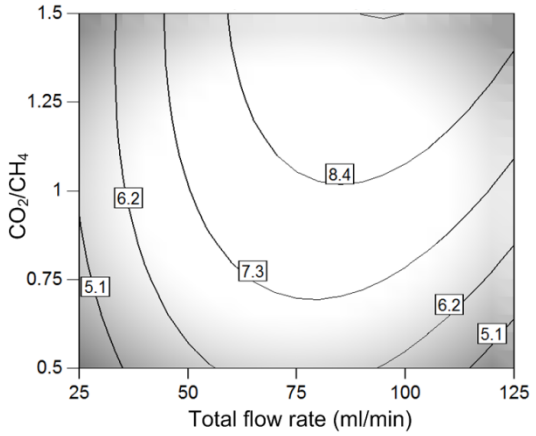

(b)

Fig. 11. Interaction between biogas flow rate and CO_2/CH_4 molar ratio on the FPE at a discharge power of 40 W and a Ni loading of 10 wt.%: (a) 3D surface plot; (b) projected contour plot.

Fig. 12 shows the combined effects of discharge power and Ni loading on the FPE. At a constant Ni loading, the FPE decreased initially with the discharge power until it reached a minimum value, and then slightly increased with the plasma power. The minimum FPE was independent of Ni loading and was achieved at a discharge power of 50 W. Moreover, to get a high FPE the optimal Ni loading was around 10 wt.%, regardless of the change of discharge power, while the maximum FPE was achieved at a discharge power of 20 W. The contour lines (see Fig. 12 (b)) showed a symmetrical shape, suggesting a weak interaction between the discharge power and Ni loading on

the FPE, which can also be evidenced by the high p-value (0.9659) of the term x_1x_4, listed in Table S5.

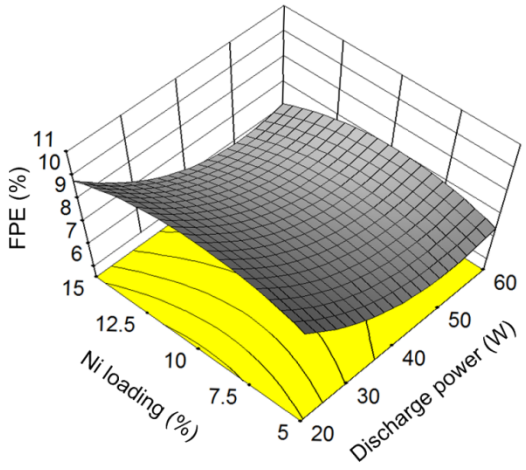

(a)

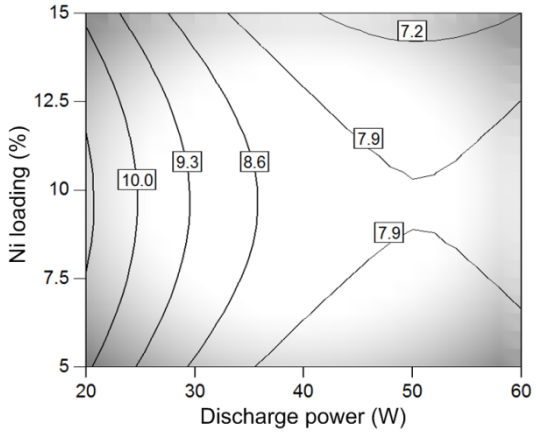

(b)

Fig. 12. Interaction between discharge power and Ni loading on the FPE at a biogas flow rate of 75 ml/min and a CO_2/CH_4 molar ratio of 1:1: (a) 3D surface plot; (b) projected contour plot.

3.2.5 Process optimization

We find that the conversion of biogas and product yield followed the same trend with respect to the process parameters. However, a trade-off between the conversion (or product yield) and FPE can be clearly seen under the same operating conditions. For example, higher biogas conversion and product yield can be achieved at a higher discharge power when the other processing parameters were kept constant. However, the corresponding FPE of the hybrid process was low at the same

conditions. By contrast, higher total biogas flow rate resulted in higher FPE but significantly decreased the conversion of biogas and the yield of products due to decreased residence time of the reactants. Fig. 13 shows the effect of SEI on the biogas conversions, product yields and FPE. Clearly, increasing the SEI enhanced both the conversions of biogas and the yield of syngas, but significantly decreased the FPE.

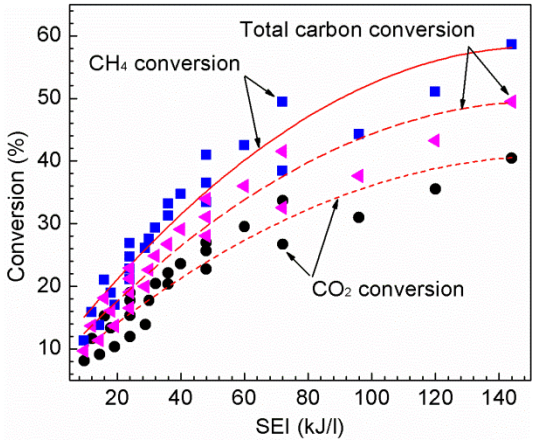

(a)

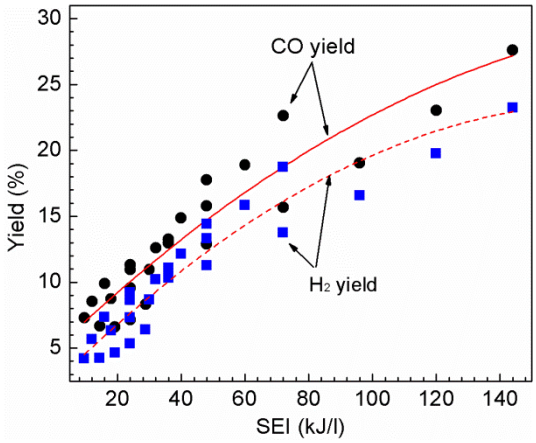

(b)

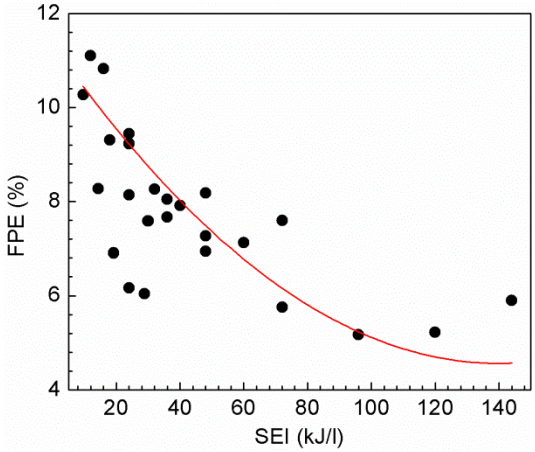

(c)

Fig. 13. Effect of SEI on reactant conversion, product yield and FPE at a CO_2/CH_4 molar ratio of 1:1 and a Ni loading of 10 wt.%.

The trade-off between the conversion of biogas and energy efficiency was also reported in previous studies [13, 15, 39-45]. Fig. 14 shows a comparison of the total carbon conversion and the FPE as a function of the SEI using different atmospheric pressure non-thermal plasma sources. For reasonable and fair comparison, only the dry reforming processes with a CO_2/CH_4 molar ratio of 1:1 using atmospheric pressure plasmas were selected. In the plasma process without a catalyst, Wang et al. reported a CO_2 conversion of 52.7% and a CH_4 conversion of 79.5% with the corresponding maximum total carbon conversion of 66.1% using a DBD at a SEI of 533 kJ/l (discharge power: 177.8 W; biogas flow rate: 20 ml/min). However, this high conversion of biogas resulted in a very low FPE of 2.7% [39]. Moreover, the maximum FPE of the plasma reforming process was 7.7% at the expense of a relatively low total carbon conversion (31.0%) in their work [39]. Similar phenomena were also observed in previous works using DBD reactors in the absence of a catalyst [40, 41]. Gliding arc has been shown very effective for dry reforming of CH_4 due to its high electron density and high flexibility to work at a relatively high reactant flow [15]. A maximum FPE of 47.2% was obtained at a SEI of 1.3 kJ/l with an input power of 165 W and a total feed flow rate of 7.5 l/min, but at a relatively lower total carbon conversion (9.8%) [15]. Eliasson et al. investigated the effect of zeolite NaX on the plasma-catalytic dry reforming of methane in a DBD reactor [42]. A maximum total carbon conversion of 55.0% was obtained at an input power of 500 W and a biogas flow rate of 150 ml/min (a SEI of 200 kJ/l), resulting in a low FPE of 2.8%; while the highest FPE of 6.4% was achieved at a significantly lower SED of 37.5 kJ/l, with a lower total carbon conversion of 17.7% [42]. Similar phenomena were also observed for the plasma-catalytic dry reforming over other zeolite catalysts, such as zeolite NaY [43], zeolite HY [44], and zeolite A [45]. Additionally, Zheng et al. prepared silica-coated $LaNiO_3$ nanoparticles ($LaNiO_3$@ SiO_2 NPs)

for the production of syngas from dry reforming of CH_4 in a DBD reactor [13]. A maximum total carbon conversion of 63.3% was obtained at a power of 160 W and a biogas flow rate of 50 ml/min (a SEI of 192 kJ/l), which corresponded to a relatively low FPE (5.9%) compared to the maximum FPE of 6.3% obtained at a lower SED of 120 kJ/l [13].

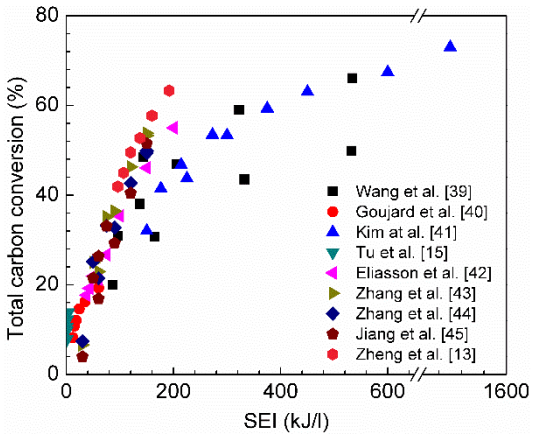

(a)

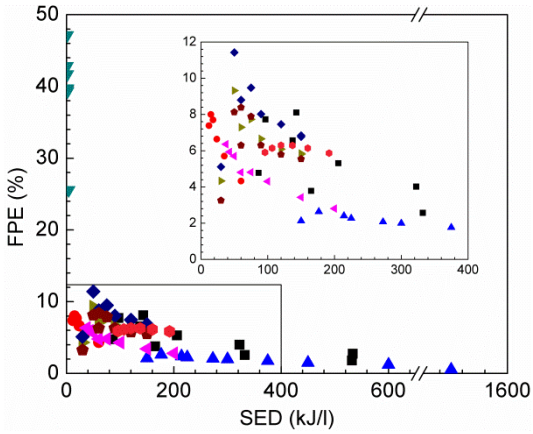

(b)

Fig. 14.Comparison of total carbon conversion and FPE vs. SEI of the reforming process using different atmospheric pressure non-thermal plasmas at a CO_2/CH_4 molar ratio of 1:1.

The trade-off between the conversion of CO_2 and CH_4 was also observed when changing the CO_2/CH_4 molar ratio in the feed gas whilst keeping the other process parameters fixed. Fig. 15 shows a comparison of biogas conversion vs. CO_2/CH_4 molar ratio using different atmospheric pressure non-thermal plasmas. In our study, increasing the CO_2/CH_4 molar ratio from 1:2 to 3:2 decreased CO_2 conversion from 23.3% to 15.8% but increased CH_4 conversion from 19.4% to

37.8%; while the corresponding total carbon conversion initially increased slightly before reaching a peak value at a CO_2/CH_4 molar ratio of 5:4 and then declining gradually. Wang et al. found that CO_2 conversion decreased from 43.6% to 27.1%, while CH_4 conversion increased by 81.8% when the CO_2/CH_4 molar ratio varied from 1:5 to 5:1 [39]. The conversions of CO_2 and CH_4 in their work were higher than our results, due to higher SED in their work (71.5 kJ/l) than that in this study (32 kJ/l).

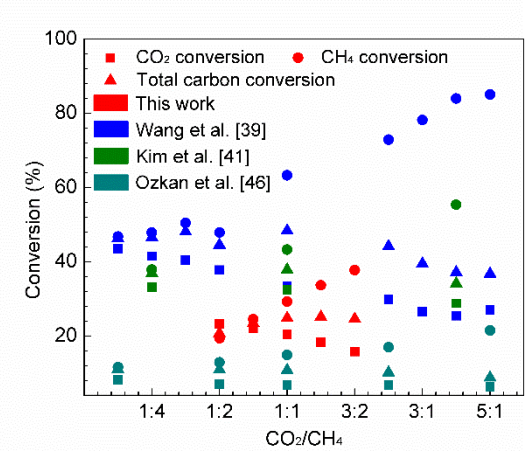

Fig. 15. Comparison of reactant conversion vs. CO_2/CH_4 molar ratio of the reforming process using different atmospheric pressure non-thermal plasmas.

The overall performance of plasma-catalytic biogas reforming strongly depends on a wide range of process parameters. In addition, a balance between biogas conversion and energy efficiency as well as a balance between CO_2 and CH_4 conversions is of significant importance for the development of an efficient plasma process for biogas reforming. Therefore, it is essential to optimize the plasma biogas reforming process using multiple inputs and responses to obtain a specified target. In this work, the aim of the process optimization was to find the combination of plasma process parameters that maximize the biogas conversion (or product yield) and FPE simultaneously. The optimal process conditions were determined by RSM coupled with function maximization approach using the regression analysis program (Design Expert 10 software, trial version) [34]. The global desirability function (D) was used to identify the optimal process

parameters and performance in the plasma-catalytic process. The optimal process parameters can be achieved when the highest value D is found.

Table 5 shows the different values of D for the plasma-catalytic biogas reforming. The optimal process performance - CO_2 conversion (31.7%), CH_4 conversion (48.1%), CO yield (21.7%), H_2 yield (17.9%) and FPE (7.9%) – can be achieved at a discharge power of 60.0 W, a total flow rate of 56.1 ml/min, CO_2/CH_4 molar ratio of 1.03 and a Ni loading of 9.5 wt.%, as the highest D value of 0.854 was obtained. To validate this predicted result, five additional experimental runs were carried out using the optimal process parameters. The results showed that the experimental results reasonably agreed with the predicted ones, with a relative error of less than 10% for all of the five responses. The reproducible results confirmed that DoE can be used to optimize the plasma-catalytic biogas reforming process. In addition, the carbon deposition on the spent Ni catalyst was only 3.9% after running the plasma-catalytic reaction under the optimal conditions for 150 min (see Fig. 16). In Fig. 16, the weight loss of the spent catalyst at around 100 ^oC was related to the desorption of moisture. The rapid weight loss of the sample at around 320 ^oC was associated with the oxidation of easily oxidized carbonaceous species, which was the active species for CO formation in the dry reforming process and did not contribute to catalyst deactivation [47]. The weight loss of the catalyst at around 450 ^oC can be ascribed to the oxidation of amorphous carbon, while the weight loss above 650 ^oC can be attributed to the oxidation of graphite carbon [47]. The deposited graphite carbon was responsible for the deactivation of catalysts [47]. The Ni/γ-Al_2O_3 catalysts used in this work showed a high stability as less deposited graphite carbon was formed, which can be confirmed by our experimental results which show that the conversion of biogas did not change significantly when running the plasma reaction for 150 min. Moreover, the carbon deposition in this study was much lower than that reported in the previous study using a similar Ni/Al_2O_3 catalyst [25].

Table 5 Optimization of plasma-catalytic biogas reforming process

Opt.	Discharge power (W)	Total flow rate (ml/min)	CO_2/CH_4 ratio	Ni loading (wt.%)	CO_2 conversion (%)	CH_4 conversion (%)	CO yield (%)	H_2 yield (%)	Fuel production efficiency (%)	D
1	60.0	56.1	1.03	9.5	31.7	48.1	21.7	17.9	7.9	0.854
2	59.9	55.8	1.04	9.6	31.7	48.1	21.7	17.9	7.9	0.852
3	59.9	55.6	1.04	10.2	31.7	48.1	21.8	17.9	7.8	0.851
4	59.6	55.5	1.04	9.3	31.7	48.1	21.7	17.9	7.8	0.850
5	60.0	53.9	1.09	10.0	31.6	50.2	22.6	18.7	7.8	0.848

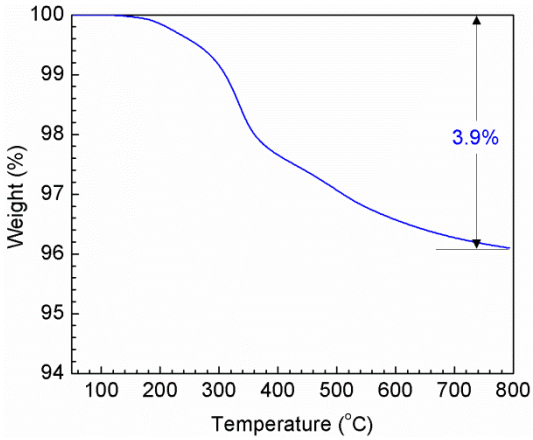

Fig. 16. TG results of the Ni catalyst (9.5 wt.% Ni/γ-Al_2O_3) after reaction under the optimum condition for 150 min.

4. Conclusions

In this study, the effects of different process parameters (biogas flow rate, discharge power, CO_2/CH_4 molar ratio and Ni loading) on the plasma CO_2 reforming of CH_4 over Ni/γ-Al_2O_3 catalyst were investigated using a CCD based RSM. Catalyst characterization (BET, XRD and TGA) was used to reveal the properties of the catalysts before and after the reaction. Regression models were established to relate the process parameters to the performance of the plasma process (e.g. conversion of biogas, yield of products and energy efficiency). The significance and adequacy of the regression models and the relative importance of these process parameters on the plasma process were evaluated by the ANOVA. The influence of the individual processing parameters and their interactions on the reaction performance was discussed in detail using the 3D response

surfaces and 2D contour plots. The XRD patterns of the fresh catalysts demonstrated that NiO was the main Ni species formed on the catalyst surface, which can be reduced in the Ar/H_2 plasma prior to plasma biogas reforming. The ANOVA results showed that the total flow rate was the most important parameter affecting the conversion of biogas and product yield, while the CO_2/CH_4 molar ratio played a dominant role in determining the energy efficiency of the plasma process. The optimum Ni loadings for achieving high reaction performance were found; however, these optimum values were slightly affected by other process parameters. The interaction between total flow rate and discharge power imposed a significant effect on all responses, while other interactions showed different influences on the responses of the plasma process. The optimal process operating conditions (discharge power of 60.0 W, total flow rate of 56.1 ml/min, CO_2/CH_4 molar ratio of 1.03 and Ni loading of 9.5 wt.%) were determined by the process optimization and validated by the reproducible experimental results under the theoretical optimal conditions. Furthermore, after running the plasma biogas reforming process under the optimum conditions for 150 min, the carbon content on the spent catalyst was 3.9%, which was lower than that reported in previous plasma-catalytic dry reforming processes using similar Ni catalysts.

Acknowledgements

The support of this work by the EPSRC SUPERGEN Hydrogen & Fuel Cell (H2FC) Programme (EP/J016454/1, Ref EACPR_PS5768), EPSRC CO2Chem Seedcorn grant and the Royal Society - Newton Advanced Fellowship (Ref. NA140303) is gratefully acknowledged.

Appendix A. Supplementary material

Electronic Supplementary Information (ESI) available: [details of regression models based on the real value of the independent variables, ANOVA for response surface quadratic models for the five responses, and the combined effect of independent variables on the responses are available]

References

[1] W.M. Budzianowski, Renew. Sustain. Energy Rev. 54 (2016) 1148-1171.

[2] EurObserv' ER Biogas barometer, 2012.

[3] M.C.J. Bradford, M.A. Vannice, Catal. Rev. 41 (1999) 1-42.

[4] J.-L. Liu, H.-W. Park, W.-J. Chung, W.-S. Ahn, D.-W. Park, Chem. Eng. J. 285 (2016) 243-251.

[5] B. Ashford, X. Tu, Current Opinion in Green and Sustainable Chemistry 3 (2017) 45-49.

[6] S. Liu, D. Mei, L. Wang, X. Tu, Chem. Eng. J. 307 (2017) 793-802.

[7] D. Mei, X. Tu, J. CO_2 Util. 19 (2017) 68-78.

[8] D.H. Mei, X.B. Zhu, Y.L. He, J.D. Yan, X. Tu, Plasma Sources Sci. Technol. 24 (2015) 015011.

[9] H. Zhang, F. Zhu, X. Li, K. Cen, C. Du, X. Tu, Chem. Eng. J. 310 (2017) 114-119.

[10] D. Mei, B. Ashford, Y.-L. He, X. Tu, Plasma Process. Polym. (2016) DOI: 10.1002/ppap.201600076.

[11] X. Tu, J.C. Whitehead, Appl. Catal. B-Environ. 125 (2012) 439-448.

[12] Y.X. Zeng, X.B. Zhu, D.H. Mei, B. Ashford, X. Tu, Catal. Today 256 (2015) 80-87.

[13] X.G. Zheng, S.Y. Tan, L.C. Dong, S.B. Li, H.M. Chen, Chem. Eng. J. 265 (2015) 147-156.

[14] Z. Bo, J.H. Yan, X.D. Li, Y. Chi, K.F. Cen, Int. J. Hydrogen Energy 33(20) (2008) 5545-5553.

[15] X. Tu, J.C. Whitehead, Int. J. Hydrogen Energy 39 (2014) 9658-9669.

[16] Q. Wang, B. Spasova, V. Hessel, G. Kolb, Chem. Eng. J. 262 (2015) 766-774.

[17] A.M. Ghorbanzadeh, S. Norouzi, T. Mohammadi, J. Phys. D Appl. Phys. 38 (2005) 3804-3811.

[18] D. Li, X. Li, M. Bai, X. Tao, S. Shang, X. Dai, Y. Yin, Int. J. Hydrogen Energy 34 (2009) 308-313.

[19] M.-W. Li, Y.-L. Tian, G.-H. Xu, Energy Fuels 21 (2007) 2335-2339.

600 [20] A. Aziznia, H.R. Bozorgzadeh, N. Seyed-Matin, M. Baghalha, A. Mohamadalizadeh, J. Nat.
601 Gas Chem. 21(4) (2012) 466-475.
602 [21] U. Kogelschatz, Plasma Chem. Plasma Process. 23 (2003) 1-46.
603 [22] D. Mei, X. Zhu, C. Wu, B. Ashford, P.T. Williams, X. Tu, Appl. Catal. B- Environ. 182
604 (2016) 525-532.
605 [23] S. Mahammadunnisa, P.M.K. Reddy, B. Ramaraju, C. Subrahmanyam, Energy Fuels 27
606 (2013) 4441-4447.
607 [24] X. Tu, H.J. Gallon, M.V. Twigg, P.A. Gorry, J.C. Whitehead, J. Phys. D Appl. Phys. 44 (2011)
608 274007.
609 [25] Q. Wang, B.-H. Yan, Y. Jin, Y. Cheng, Energy Fuels 23 (2009) 4196-4201.
610 [26] X. Zhu, X. Tu, D. Mei, C. Zheng, J. Zhou, X. Gao, Z. Luo, M. Ni, K. Cen, Chemosphere 155
611 (2016) 9-17.
612 [27] D. Mei, Y.-L. He, S. Liu, J. Yan, X. Tu, Plasma Process. Polym. 13 (2016) 544-556.
613 [28] W. Wang, A. Berthelot, S. Kolev, X. Tu, A. Bogaerts, Plasma Sources Sci. Technol. 25 (2016)
614 065012.
615 [29] C. De Bie, T. Martens, J. van Dijk, S. Paulussen, B. Verheyde, S. Corthals, A. Bogaerts,
616 Plasma Sources Sci. Technol. 20 (2011) 024008.
617 [30] R. Snoeckx, R. Aerts, X. Tu, A. Bogaerts, J. Phys. Chem. C 117 (2013) 4957-4970.
618 [31] C. De Bie, J. van Dijk, A. Bogaerts, J. Phys. Chem. C 119 (2015) 22331-22350.
619 [32] M.A. Bezerra, R.E. Santelli, E.P. Oliveira, L.S. Villar, L.A. Escaleira, Talanta 76 (2008) 965-
620 977.
621 [33] D.C. Montgomery, Design and Analysis of Experiments, Wiley, New York, 2012.
622 [34] Design-Expert® Software Version 10: http://www.statease.com/dx10.html
623 [35] Y.K. Han, C.-I. Ahn, J.-W. Bae, A.R. Kim, G.Y. Han, Ind. Eng. Chem. Res. 52 (2013) 13288-
624 13296.
625 [36] X. Tu, H.J. Gallon, J.C. Whitehead, Catal. Today 211 (2013) 120-125.

626 [37] A.-J. Zhang, A.-M. Zhu, J. Guo, Y. Xu, C. Shi, Chem. Eng. J. 156 (2010) 601-606.
627 [38] H.L. Liu, Y.R. Chiou, Chem. Eng. J. 112 (2005) 173-179.
628 [39] Q. Wang, B.H. Yan, Y. Jin, Y. Cheng, Plasma Chem. Plasma Process. 29(2009) 217-228.
629 [40] V. Goujard, J.-M. Tatibouet, C. Batiot-Dupeyrat, Plasma Chem. Plasma Process. 31 (2011)
630 315-325.
631 [41] T.K. Kim, W.G. Lee, J. Ind. Eng. Chem. 18 (2012) 1710-1714.
632 [42] B. Eliasson, C.J. Liu, U. Kogelschatz, Ind. Eng. Chem. Res. 39 (2000) 1221-1227.
633 [43] K. Zhang, U. Kogelschatz, B. Eliasson, Energy Fuels 15 (2001) 395-402.
634 [44] K. Zhang, B. Eliasson, U. Kogelschatz, Ind. Eng. Chem. Res. 41 (2002) 1462-1468.
635 [45] T. Jiang, Y. Li, C.J. Liu, G.H. Xu, B. Eliasson, B.Z. Xue, Catal. Today 72 (2002) 229-235.
636 [46] A.Ozkan A, T. Dufour, G. Arnoult, P. de Keyzer, A. Bogaerts, F. Reniers, J. CO_2 Util. 9
637 (2015) 74-81.
638 [47] L.M. Zhang, L. Li, Y.H. Zhang, Y.X. Zhao, J.L. Li, J. Energy Chem. 23 (2014) 66-72.
639
640